Neurexophilin 3 is highly localized in cortical and cerebellar regions and is functionally important for sensorimotor gating and motor coordination

MOLECULAR AND CELLULAR BIOLOGY, Aug. 2005, p. 7278–7288 Vol. 25, No. 16
0270-7306/05/$08.00+0 doi:10.1128/MCB.25.16.7278–7288.2005

Neurexophilin 3 Is Highly Localized in Cortical and Cerebellar Regions and Is Functionally Important for Sensorimotor Gating and Motor Coordination

Vassilios Beglopoulos,[1]† Monique Montag-Sallaz,[2] Astrid Rohlmann,[1] Kerstin Piechotta,[1] Mohiuddin Ahmad,[1] Dirk Montag,[2] and Markus Missler[1,3]*

Center for Physiology and Pathophysiology, Georg-August University, Göttingen, Germany[1]; Neurogenetics Research Group, Leibniz Institute for Neurobiology, Magdeburg, Germany[2]; and Department of Genetics and Molecular Neurobiology, Institute of Biology, Otto-von-Guericke-University, Magdeburg, Germany[3]

Received 11 March 2005/Returned for modification 26 April 2005/Accepted 1 June 2005

Neurexophilin 3 (Nxph3) is a specific ligand of synaptic α-neurexins that are essential for efficient neurotransmitter release. Previous biochemical work demonstrated that Nxph3 interacts with an extracellular domain of α-neurexins in a tight complex; however, no information is available on the localization or functional role of Nxph3 in the brain. Here, we generated *lacZ* reporter gene knock-in mice to investigate the distribution of Nxph3 at the single-cell level and Nxph3 knockout mice to examine its functional importance. Nxph3 expression was restricted mostly to subplate-derived neurons in cortical layer 6b, granule cells in the vestibulocerebellum, and Cajal-Retzius cells during development. Colabeling experiments demonstrated that neurons expressing Nxph3 do not belong to a uniform cell type. Morphological analyses and systematic behavioral testing of knockout mice revealed no anatomical defects but uncovered remarkable functional abnormalities in sensory information processing and motor coordination, evident by increased startle response, reduced prepulse inhibition, and poor rotarod performance. Since Nxph3-deficient mice behaved normally while performing a number of other tasks, our data suggest an important role for Nxph3 as a locally and temporally regulated neuropeptide-like molecule, presumably acting in a complex with α-neurexins in select neuronal circuits.

Synapses differ widely in their structural and physiological properties. The synaptic transmembrane proteins α- and β-neurexin, in concert with their binding partners, including neurexophilins, have been proposed to be involved in underlying molecular mechanisms (9, 11, 17, 19, 20, 28, 31, 36). We have recently reported an essential role for α-neurexins at synapses (21), in line with their property as presynaptic α-latrotoxin receptors (8, 30) and their widespread expression in virtually all neurons (35). In α-neurexin knockout mice, neurotransmitter release is strongly reduced due to an impaired function of high-voltage activated Ca^{2+} channels (21). This role of α-neurexins specifically affects N- and P/Q-type Ca^{2+} channels and requires α-neurexin-specific extracellular sequences which cannot be replaced by the much shorter extracellular sequences of β-neurexins (40), indicating that extracellular protein-protein interactions may be involved. Consistent with the apparent functional specialization of α- and β-neurexins (4, 21), biochemical data have identified different extracellular interaction partners for these major neurexin isoforms (11, 18, 31).

Neurexophilins are tightly bound extracellular ligands of α-neurexins that can be separated only under near-denaturing conditions (24, 25), suggesting that neurexophilin function involves the formation of a complex with α-neurexins. Neurexophilins comprise a family of four glycoproteins (Nxph1 to Nxph4) that exhibit the characteristics of secreted, preproprotein-derived molecules (7, 20, 26), and orthologues can be found only at the vertebrate level. Previous studies demonstrated that in rats and mice, only Nxph1 and Nxph3 interact biochemically with α-neurexins and that the second LNS domain in α-neurexins is sufficient to mediate this binding (18). In contrast, Nxph2 is expressed only in humans (7, 20, 26), and Nxph4 does not bind to α-neurexins, since the conserved domains are connected by a different linker region (18). Furthermore, in situ hybridization data suggested that Nxph1 is present in many inhibitory interneurons (26), and a preliminary knockout analysis of Nxph1 indicated that it is not an essential gene for mouse survival (18). However, these previous studies provided no information on the localization or functional role of Nxph3 in the brain. Such data are essential to distinguish between the following alternative hypotheses on the putative role of these molecules: (i) if Nxph3 expression is widespread and its deletion produces a strong phenotype, similar to that of the α-neurexin mutants, Nxph3 would seem to serve as a generally required cofactor of α-neurexins, as suggested by their tight interaction, and (ii) if Nxph3 distribution is restricted and its deletion affects only neuronal subpopulations, Nxph3 would be likely to perform a more independent and possibly modulatory role, as suggested by the evolutionarily late appearance at the vertebrate level.

Here, we first generated knock-in mice coexpressing *lacZ* from the Nxph3 locus, overcoming the lack of isoform-specific

* Corresponding author. Mailing address: Center for Physiology and Pathophysiology, Georg-August University, Humboldtallee 23, Göttingen D-37073, Germany. Phone: 49-551-3912807. Fax: 49-551-3912809. E-mail: mmissle1@gwdg.de.

† Present address: Center for Neurologic Diseases, Brigham and Women's Hospital, Harvard Medical School, Boston, MA 02115.

antibodies and improving the cellular resolution beyond that seen with conventional hybridization. Prominent Nxph3 expression was restricted mostly to (i) layer 6b of the cerebral cortex, where it occurs in subplate-derived excitatory neurons; (ii) granule cells in the vestibulocerebellum; and (iii) Cajal-Retzius cells during development. We then converted Nxph3-*lacZ* knock-in mice into null mutants using the *cre-loxP* system. Due to the restricted expression pattern of Nxph3 that impedes straightforward electrophysiological approaches, we evaluated its functional significance using behavioral analysis. Nxph3 knockout mice showed impaired sensory information processing and motor coordination. These abnormalities can be traced back to neuronal circuits that normally contain Nxph3, i.e., the confined cortical and cerebellar regions revealed by the knock-in analysis. In contrast, morphological experiments failed to show any structural deficiencies in the brains of knockout animals. Our data suggest that Nxph3 plays a role as an important modulator molecule in a subpopulation of neurons, presumably acting in a tight complex with presynaptic α-neurexins at select synapses.

MATERIALS AND METHODS

Generation of *lacZ* knock-in mice. A 570-bp-long NheI-SfiI fragment from rat Nxph3 cDNA (20) was used to screen a λ phage genomic library from 129SvJ mice (Stratagene). Two genomic clones (17.3-kb pmλNxph3-2 and 6.5-kb pmλNxph3-3) were characterized, and a knock-in targeting vector was constructed in four steps to facilitate the subsequent generation of a null mutant allele by *cre-loxP*-based excision (29), as follows: (i) By using PCR-based mutagenesis, the stop codon of Nxph3 was replaced by a BamHI site. (ii) A marker cassette was inserted into the BamHI site, consisting of a tandem Flag tag, a stop codon, a bicistronic entry site (internal ribosome entry site [IRES]) (23), a *lacZ* sequence together with a nuclear localization signal, and the 34-bp-long *loxP* site 3′ of the exon. (iii) The 5′ loxP site, followed by the selection marker, was introduced into an NcoI site between the first and second coding exon. Additionally, the Neo^R sequence was flanked by FRT sites to allow subsequent removal using Flp recombinase, if necessary (6). (iv) The assembled sequence containing both coding exons, the marker and selection cassettes, and flanking intronic regions was finally inserted into a targeting vector backbone that contained two thymidine kinase modules as negative selector. As an alternative step (iv), the same fragment was subcloned into a mammalian expression vector (pCMV5). Embryonic stem cell line 14.1 was maintained under standard conditions (using fetal calf serum from Perbio-HyClone and ESGRO-LIF from Chemicon) on mouse embryonic fibroblasts inactivated with 10 μg/ml mitomycin C (Sigma). Clones doubly resistant to G418 (190 μg/ml active compound) and ganciclovir (0.25 μM) were selected, and two homologous recombinants (59 and 73; see Results) were selected for blastocyst injection, giving rise to independent knock-in mouse lines maintained on a 129SvJ × C57BL/6J hybrid background.

Creation of knockout mice and genotyping. Knockout mice were generated by crossing floxed knock-in mice to Cre recombinase-expressing EIIa $Cre^{+/tg}$ transgenic animals (15). This strategy effectively deleted the second exon and all exogenous sequences except a single *loxP* site. Knock-in and knockout animals were initially characterized by Southern blot analysis (see Results). The lineages were then genotyped mainly by PCR, using the following oligonucleotides: for the wild-type (WT) allele, 01-65 (5′-CACGGACTATCGACTGGTGCA GAAG) versus 01-67 (5′-GACCGAGAGTCATGACAGCAAACAC), with a product length of 600 bp; for the knock-in allele, 01-64 (5′-CCAGATTACAAC TACCACAGTGATAC) versus 01-66 (5′-GAAGTACATGAGCGGATAACG GATC), with a product length of 370 bp; for the knockout allele, 00-19 (5′-GA GCCTCCCATCCCAGCTCCTCAG) versus 00-24 (5′-CTAACCTCAGGTTG GGCACAGCAC), with a product length of 400 bp; and for the Cre allele, 1304 (5′-CCAGGCTAAGTGCCTTCTCTACA) versus 1303 (5′-AARGCTTCTGTC CGTTTGCCGGT), with a product length of 500 bp.

Biochemical and molecular biological procedures. COS-7 cells were maintained and transfected using the DEAE-dextran method essentially as described previously (20). β-Galactosidase activity was visualized with X-Gal (5-bromo-4-chloro-3-indoyl-β-D-galactopyranoside) staining solution (1 mg/ml X-Gal, 2 mM $MgCl_2$, 5 mM potassium ferricyanide, and 5 mM potassium ferrocyanide in phosphate-buffered saline [PBS]) at 37°C for 4 h. For immunoblotting, transfected cells were lysed with 1% NP-40, and protein samples were analyzed by sodium dodecyl sulfate-polyacrylamide gel electrophoresis and enhanced chemiluminescence detection, using a commercial antibody against the Flag epitope (M2; Sigma), polyclonal antisera to neurexophilins (F508; cross-reactive to Nxph1 and Nxph3), and neurexins (A473) reported previously (26). Pulldown experiments with α-neurexin enriching for bound Nxphs were performed with recombinant α-latrotoxin immobilized on CNBr-activated Sepharose beads using 2% Triton X-100 extracted brain homogenates (buffer of 20 mM Tris [pH 7.5], 80 mM NaCl, 2.5 mM $CaCl_2$, and 100 μg/ml phenylmethylsulfonyl fluoride) from control and knockout mice, essentially as described previously (18). Total RNA was extracted from brains of Nxph3 knock-in and control mice (RNeasy II; QIAGEN). The reverse transcription (RT)-PCR strategy was based on a common 5′ oligonucleotide primer in sense orientation (01-63, 5′-GCCAAGGTAA CATCTCCATCAGC) and two different antisense primers, one specific for the wild-type sequence corresponding to the C terminus of Nxph3 (01-57, 5′-GTA TCACTGTGGTAGTTGTAATCTGC) and the other specific for the Flag-tagged mutated allele (01-62, 5′-GTCCTTGTAGTCGCCGGCCTTGTC). Northern blotting experiments were performed with total RNA samples (RNA-Zol; WAK, Germany) from knock-in, knockout, and control mice of different developmental stages by using probes for Nxph3 as described before (20).

Morphological techniques. Mouse brains were fixed with 4% paraformaldehyde in 0.1 M phosphate buffer. Sixty-micrometer serial sections were cut at coronal or sagittal orientations and incubated with X-Gal staining solution (1 mg/ml X-Gal, 2 mM $MgCl_2$, 5 mM potassium ferricyanide, and 5 mM potassium ferrocyanide in PBS) at 37°C for 4 to 24 h to detect β-galactosidase activity. For immunohistochemistry, free-floating 30-μm sections were blocked in 10% bovine serum albumin-PBS buffer and incubated at 4°C overnight with antibodies to the following proteins: Synapsin, VGlu1, VGlu2, VGAT (Synaptic Systems, Göttingen, Germany), GAD67, Calretinin (Chemicon, Temecula), Parvalbumin (Swant, Bellinzona, Switzerland), Substance P, Somatostatin (Sigma-Aldrich), Tbr1, and Reelin (clone G10). Secondary antibodies for peroxidase/diaminobenzidine detection were from Sternberger Monoclonal Antibodies, Inc. In case of double-labeling with β-Gal and antibodies, 30-μm sections were first incubated in X-Gal solution and then subjected to the immunohistochemical procedure. Nissl staining was performed on 30-μm-thick serial sections using 0.1% cresyl violet acetate. In situ hybridization followed established procedures for [α-^{33}P]UTP (Amersham)-radiolabeled antisense riboprobes (T7 labeling kit; Promega) using the 570-bp NheI/SfiI fragment from Nxph3 cDNA (20). Sections were processed with emulsion autoradiography and counterstained with cresyl violet stain. All images were acquired with an Axioscope 2 microscope (Zeiss, Germany) connected to a digital camera (AxioCam HRc; Zeiss, Germany). The overview pictures in Fig. 1, 2, and 5 are composites of 6 to 10 individual captions. Quantitation of structural parameters was performed by using AxioVision software (Zeiss, Germany).

Mouse husbandry. Mice were kept under standard conditions with free access to food and water in a cycle of 12 h of light and 12 h of dark. Heterozygous parent animals ($Nxph^{+/-}$) that had already undergone more than 13 generations in a mixed 129SvJ × C57BL/6 × FVB background were bred to generate Nxph3 knockout mice and their wild-type littermate controls. One week prior to behavioral testing, mice were removed from the central facility and housed individually.

Behavioral analysis. Sex- and age-matched littermate wild-type mice were used as controls. Mice were tested during the light phase of the light/dark cycle; investigators were unaware of their genotypes. Animals were subjected to a series of behavioral tests (22, 27). General parameters indicative of health and neurological state were addressed following the neurobehavioral examination described by Whishaw et al. (38) and tests of the primary screen of the SHIRPA protocol except startle response (22, 27). Behavioral paradigms were conducted in sequential order, as follows.

(i) Grip strength. Grip strength was measured with a high-precision force sensor to evaluate neuromuscular functioning (Technical and Scientific Equipment GmbH [TSE], Bad Homburg, Germany).

(ii) Rotarod performance. Animals received two training sessions (3-h interval) on a rotarod apparatus (TSE) with the speed increasing from 4 to 40 rpm for 5 min. After 4 days, mice were tested at constant speeds of 16, 24, 32, and 40 rpm. The latency for falling off the rotating rod was measured.

(iii) Open field. Exploration was assessed by placing mice in the middle of a 50- by 50-cm arena (for 15 min). Using the VideoMot 2 system (TSE) and Wintrack software (39), tracks were analyzed for path length, visits, and relative time spent in different compartments and to determine walking speed, latency for moving, time moving or resting, and number of stops and rests.

(iv) Light-dark avoidance. Anxiety-related behavior was tested by placing mice in a brightly lit compartment (250 lx; 25 by 25 cm) adjacent to a dark compart-

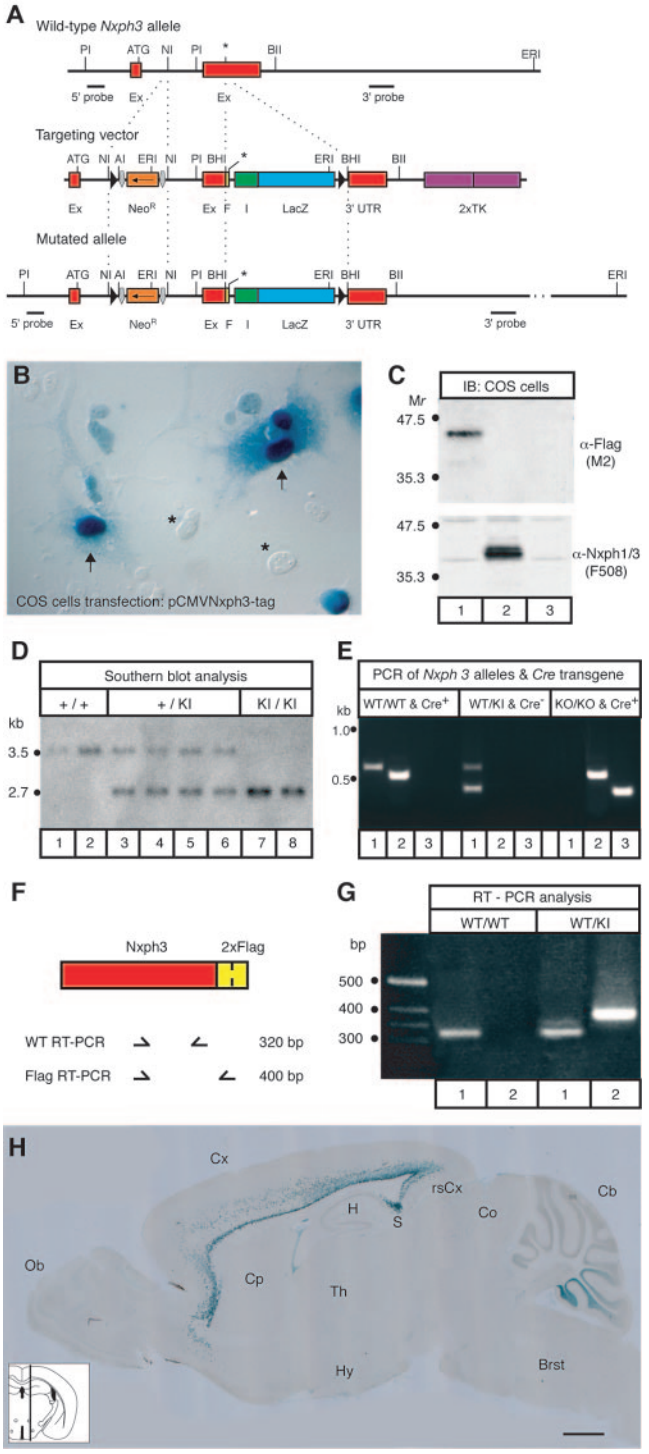

FIG. 1. Generation of Nxph3-*LacZ* reporter gene knock-in mice. (A) Knock-in strategy. ATG, start codon; Ex, coding exon; *, stop codon; Neo^R, neomycin resistance gene; F, Flag epitope; I, internal ribosomal entry site; LacZ, β-galactosidase coding sequence; 3′ UTR, 3′ untranslated region; TK, thymidine kinase; triangles, loxP sites; gray arrows, FRT sites; 5′ and 3′ probes, outside Southern probes. Abbreviations for restriction enzymes are as follows: AI, AgeI; BHI, BamHI; BII, BglII; ERI, EcoRI; NI, NcoI; and PI, PstI. (B) COS-7 cells transfected with the Nxph3 targeting sequence show enrichment of staining over nuclei as predicted (arrows). Untransfected cells (asterisks) show no staining. (C) Immunoblot analysis of COS-7 cells transfected with the Nxph 3 targeting sequence (lane 1), an untagged Nxph3 expression plasmid (lane 2), or mock-transfected (lane 3). Blots were probed with an antibody to the Flag epitope (upper panel), identifying the Nxph3-Flag fusion protein as predicted from the results shown in panel A. A peptide antiserum (lower panel) directed against the 10 C-terminal amino acid residues detects expression of the untagged Nxph3 (lane 2), but fails to recognize the Nxph3-Flag fusion protein (lane 1). (D) Southern blot analysis of PstI/AgeI-digested genomic DNA of wild-type (lanes 1 and 2), heterozygous (lanes 3 to 6), and homozygous (lanes 7 and 8) knock-in mice probed with the 5′ outside probe. (E) Short genomic PCRs used for genotyping wild-type (lanes 1, 600-bp band), knock-in (lanes 1, 400-bp band), and knockout alleles (lanes 3) and Cre transgene (lanes 2) in various combinations. (F and G) Position of oligonucleotide primers (F) and results (G) of an RT-PCR strategy to demonstrate expression of wild-type (lanes 1) and Flag epitope-tagged (lanes 2) Nxph3 mRNA in the brain. (H) Overview of a parasagittal section (see inset) from a 20-day-old knock-in mouse processed for β-galactosidase histochemistry, resulting in a blue reaction product where Nxph3 is expressed. Brst, brainstem; Cb, cerebellum; Co, colliculi; Cp, caudate putamen; Cx, cortex; H, hippocampal formation; Hy, hypothalamus; Ob, olfactory bulb; rsCx, retrosplenial cortex; S, subiculum; Th, thalamus. Bar, 800 μm.

ment (12.5 by 25 cm). The numbers of transitions between the two compartments were analyzed during 10-min test sessions.

(v) Morris water maze. Spatial learning was assessed by using a hidden platform version of the Morris task. Mice were allowed to swim until they found the platform or until 120 s had elapsed. The animals underwent six trials per day during 5 consecutive days with the platform positioned in the southeast quadrant during the first 3 days (total of 18 trials; acquisition phase) and in the opposite quadrant for the last 2 days (total of 12 trials; reversal phase). Trials 19 and 20 were defined as probe trials to analyze the precision of spatial learning.

(vi) Two-way active avoidance learning. A two-chambered shuttle box (TSE) was used to assess associative learning. During the conditioning stimulus (CS; 10 s of light), the animals had to move to the dark side of the shuttle box to avoid an electrical shock to the feet (unconditioned stimulus [US]; 5 s, 0.3 mA pulsed) delivered after the CS. The mice were tested during 5 consecutive days with 80 trials per day, and the 5- to 15-s intertrial interval varied stochastically. Compartment changes during presentation of the CS were counted as conditioned (correct) avoidance reactions and compared between groups.

(vii) Acoustic startle response and prepulse inhibition (PPI). A startle stimulus (50 ms, 120 dB) was delivered to the mice in a startle box system (TSE) with or without a preceding prepulse stimulus (30 ms, 100 ms before the startle stimulus) at eight different intensities (73 to 94 dB, 3-dB increments) on a 70-dB white-noise background. After habituation to the box (3 min), two startle trials were followed in random order by 10 startle trials and 5 trials at each of the prepulse intensities with stochastically varied intertrial intervals (5 to 30 s). The maximal startle amplitude was measured by a sensor platform.

Statistical analysis. Behavioral data were analyzed using one-way analysis of variance (ANOVA) with genotype as a factor and post hoc with Scheffe's test (StatView program; SAS Institute Inc., Cary, NC). In addition, for the rotarod, open field, water maze, two-way active avoidance, and startle/PPI experiments, statistical analysis was performed using repeated measures ANOVA (with genotype as the between-subject factor and session as the within-subject factor).

RESULTS

Nxph3 expression is highly localized in distinct brain regions. To localize Nxph3 in the absence of specific antibodies, we used an alternative neurogenetic approach. Since the Nxph3 gene is relatively small (gene size, 4.4 kb; data not shown), we designed a knock-in strategy that could be tested in vitro. The defining component of the targeting vector (Fig. 1A) is a marker cassette that simultaneously introduced (i) a *lacZ* reporter gene sequence that should be coexpressed with *Nxph3* from its endogenous locus via a bicistronic entry site (IRES), and (ii) a tandem Flag epitope tag fused to the C terminus of Nxph3. This cassette should allow parallel localization of expressing cells (by β-galactosidase histochemistry) and of the

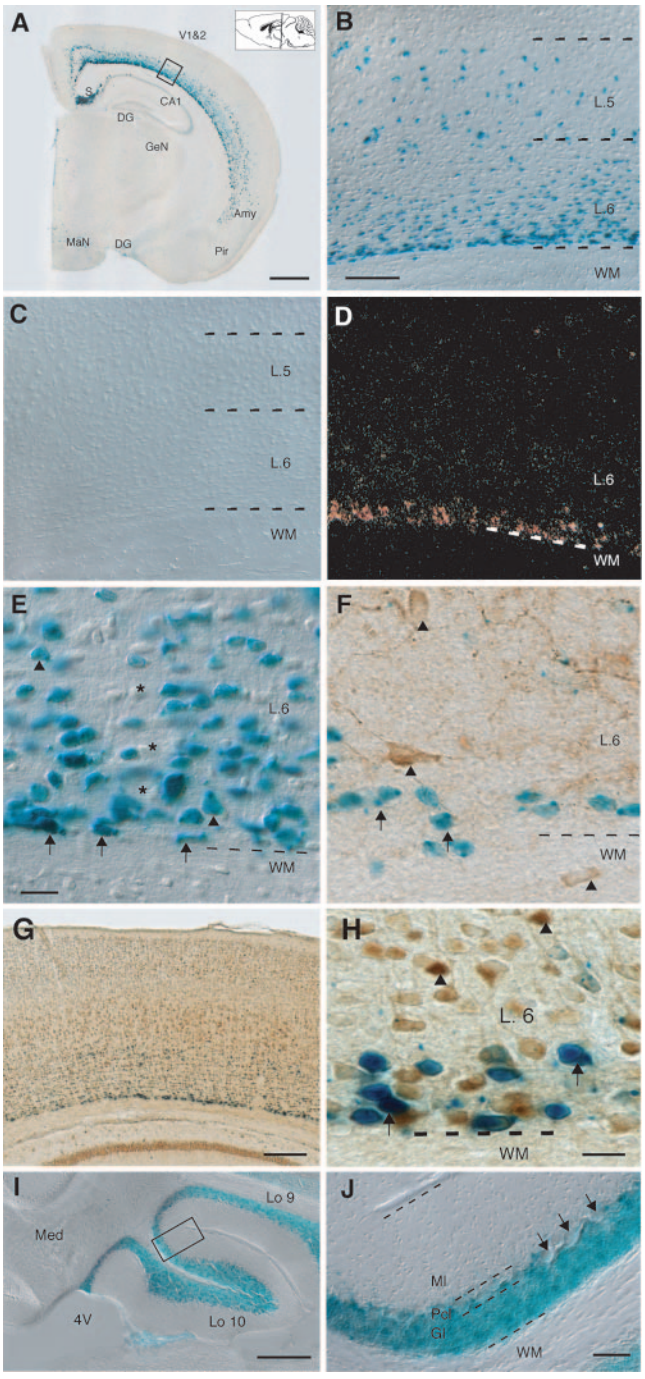

FIG. 2. Nxph3 expression is highly localized in cortical and cerebellar regions. (A) Overview picture of a coronal section (see inset) from an adult Nxph3 knock-in mouse. Prominent β-galactosidase staining is seen over deep layers of isocortical areas (e.g., visual cortex, V1&2), in the subiculum and part of the amygdala (Amy, basolateral nucleus). CA1, CA1 region of the hippocampus; DG, dentate gyrus; GeN, geniculate nucleus; MaN, mammilary nucleus; Pir, piriform cortex. Bar, 800 μm. (B) Differential interference contrast picture of the area boxed in panel A. β-Galactosidase-positive cells are enriched in layer 6 (L.6) along the border to the white matter (WM). (C) Control section from a wild-type mouse processed for β-galactosidase histochemistry. (D) Dark-field picture of an in situ hybridization experiment visualizing Nxph3 on a cortical section from an adult wild-type mouse. Bar, 150 μm (for panels B to D). (E) Overall morphology of β-galactosidase-stained cells in the cortex include horizontally oriented fusiform neurons (arrows) and medium-sized pyramidal neurons (arrowheads). Asterisks indicate neurons without Nxph3 expression. Bar, 30 μm. (F) Double-staining experiment using β-galactosidase histochemistry and antibodies against glutamate decarboxylase, GAD67. (G and H) Partial colabeling of Nxph3 with tbr1 shown at low (G) and high (H) magnification (arrows). Note that more neurons in layer 6 are Tbr1-positive (arrowheads). Bar, 30 μm. (I) Parasagittal section through parts of the cerebellar vermis from 20-day-old Nxph3 knock-in mice. Lo 10, uvula; Lo 9, nodule; Med, medial cerebellar nucleus; 4V, fourth ventricle. Bar, 200 μm. (J) Higher magnification of the area boxed in panel I demonstrates that Nxph3 is expressed by cells of the granule cell layer but appears to spare Purkinje neurons (arrows). Ml, molecular layer; Pcl, Purkinje cell layer; Gl, granule cell layer; WM, white matter. Bar, 40 μm.

Nxph3 protein itself (by antibodies against the Flag epitope). Expression of both β-galactosidase and Flag was verified with cell culture by cloning the targeting sequence under a cytomegalovirus promoter (Fig. 1B and C). Nxph3 knock-in mice were then generated, genotyped by Southern (Fig. 1D) and PCR (Fig. 1E) strategies, and obtained in the expected Mendelian ratio. Homozygous Nxph3 knock-in mice were viable and fertile, displaying no apparent abnormalities (data not shown). RT-PCR confirmed specific expression of Nxph3-Flag mRNA in brains of knock-in animals (Fig. 1F and G), but the Flag epitope was undetectable in mouse brains by immunolabeling procedures (data not shown), probably reflecting the low levels of Nxph3 in the brain. In contrast, the reporter gene strategy proved to be effective, and Nxph3-*lacZ* knock-in mice were successfully used for studying the detailed spatial and temporal distribution of Nxph3-expressing neurons. To study the expression pattern of Nxph3 in the central nervous system, serial brain sections of adult knock-in mice were processed for β-galactosidase histochemistry. As shown in the overview in Fig. 1H, Nxph3 was present in only a limited number of brain regions within the cerebral cortex and cerebellum.

The expression of Nxph3 extended over almost the entire cortex, including all isocortical areas and some but not all allocortical regions. In the latter, distinct expression was present in postcingular and retrosplenial cortices, in the presubiculum and subiculum, whereas the olfactory, piriform, and hippocampal cortices of adult mice showed virtually no expression (Fig. 2A and data not shown). In isocortical areas, Nxph3 was restricted to neuronal subpopulations, with highest levels near the border between gray and white matter. Many β-galactosidase-positive neurons were present in layer 6 (Fig. 2B), with dense clusters in sublamina 6b. While Nxph3-expressing cells constituted the majority of neurons in layer 6b, fewer positive cells were found in layer 5 (Fig. 2B). To verify that the knock-in approach reflected the actual Nxph3 distribution, we demonstrated that (i) control sections from wild-type mice showed no β-galactosidase activity (Fig. 2C); (ii) a second knock-in mouse line gave very similar results (data not shown); and (iii) the expression pattern found with knock-in mice was comparable to in situ hybridization data from wild-type mice (Fig. 2D), which confirmed the distribution for the most intensely labeled area (Fig. 2D, layer 6). A comparison of β-galactosidase staining and in situ hybridization results demonstrated the superior resolution of the knock-in approach, at least for low-abundance molecules, such as Nxph3.

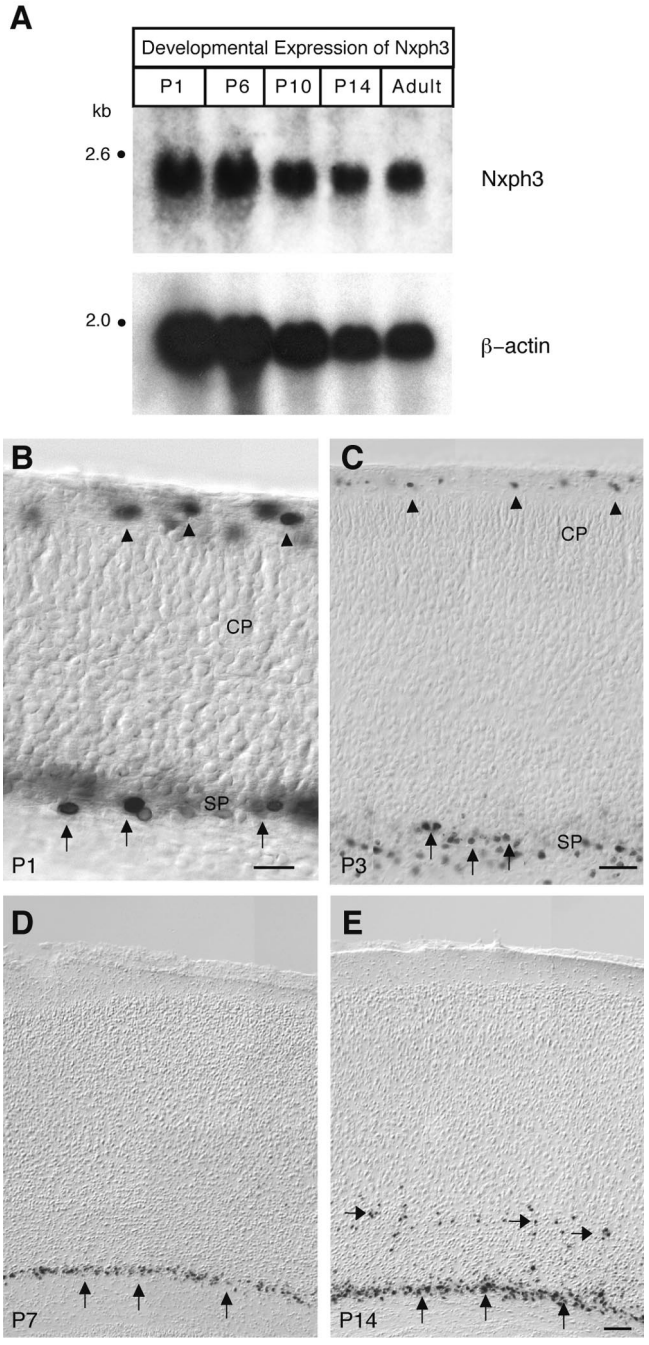

FIG. 3. Nxph3 expression in cortical brain regions during development. (A) Northern blots of brains from wild-type mice at postnatal day 1 (P1), 6 (P6), 10 (P10), and 14 (P14) and at about 6 weeks (adult). RNA samples were probed for Nxph3, and β-actin for input control. (B to E) β-Galactosidase-stained sections (pictures converted to gray scale) through the cerebral cortex from Nxph3 knock-in mice at the indicated ages. Arrowheads point to transiently expressing cells in the marginal zone, vertical arrows mark a population of subplate neurons which develops into mature layer 6 neurons after the first week, and horizontal arrows identify a few scattered neurons in layer 5 that appear last. CP, cortical plate; SP, subplate. Bars, 20 μm (B), 50 μm (C), and 100 μm (E, for panels D and E).

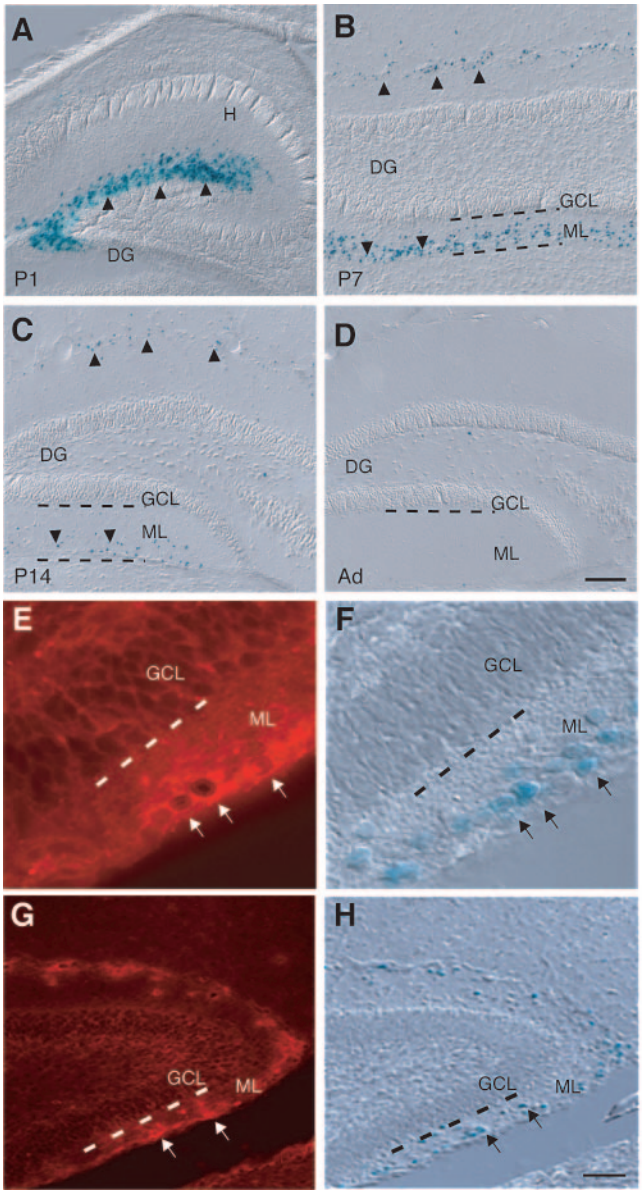

FIG. 4. Hippocampal Cajal-Retzius cells transiently expressing Nxph3. (A to D) Coronal sections through the dentate gyrus (DG) and hippocampus (H) of Nxph3 knock-in mice at the indicated ages. β-Galactosidase staining shows Nxph3-expressing cells mostly in the outer half of the molecular layer (ML) during the first postnatal week that gradually disappear afterwards. GCL, granule cell layer of the dentate gyrus. Bar in panel D (for panels A to D), 150 μm. (E and F) Double-staining of the dentate gyrus from a 7-day-old knock-in mouse with an antibody to reelin (immunofluorescence) (E) and with β-galactosidase histochemistry (differential-interference contrast) (F). The extracellular matrix protein reelin is distributed predominantly around β-Gal-positive cells in the molecular layer (ML; arrows), whereas no reelin staining can be seen over the granule cell layer (GCL). (G and H) Similar experiment using antibodies against calretinin, also showing colocalization with Nxph3-expressing cells (arrows). Bars, 30 μm (E and F) and 80 μm (G and H).

A detailed analysis showed that Nxph3-positive neurons in layer 6 of cortical areas have fusiform (Fig. 2E, arrows) or pyramidal (Fig. 2E, arrowheads) shapes in horizontal or vertical orientations, respectively. High-magnification micrographs

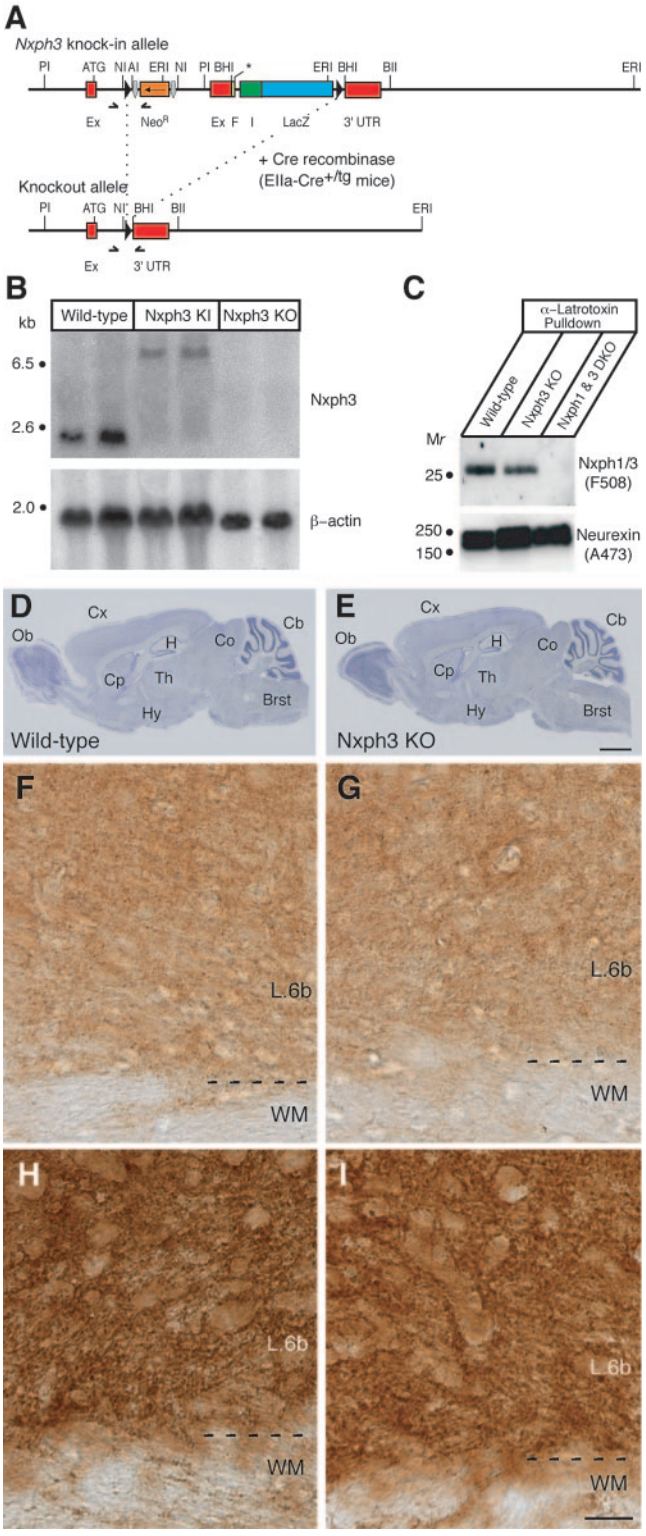

FIG. 5. Generation of Nxph3 knockout mice reveals no effect of Nxph3 on brain structure. (A) Diagram depicting the strategy of generating Nxph3 knockout mice. Primer pairs for genotyping knock-in and knockout mice are indicated by the half-arrows (for genotyping samples, see Fig. 1E). Abbreviations are as defined in the legend to Fig. 1A. (B) Northern blots of wild-type, Nxph3-*lacZ* knock-in, and Nxph3 knockout mouse brains incubated with Nxph3 probe and β-actin as the loading control. The shift to a higher-molecular-weight mRNA species in knock-in mice reflects the cotranscription of the IRES-*lacZ* cassette with Nxph3. (C) Neurexophilins were enriched from the brains of wild-type, Nxph3 knockout (KO), and Nxph1 and Nxph3 double knockout mice (Nxph1 and 3 DKO) on immobilized α-latrotoxin by virtue of their tight binding to α-neurexins. The immunoblot demonstrates the precipitation of α-neurexins (lower panel) but the complete absence of Nxph1 and Nxph3 in double knockout brains (upper panel). In Nxph3 knockout mice, the remaining band is due to the cross-reactivity with Nxph1 (18, 26), which is still present in Nxph3 null mutants. (D and E) Overview pictures of Nissl-stained parasagittal sections from brains of adult wild-type and Nxph3 knockout mice. Brst, brainstem; Cb, cerebellum; Co, colliculi; Cp, caudate putamen; Cx, cortex; H, hippocampal formation; Hy, hypothalamus; Ob, olfactory bulb; Th, thalamus. Bar, 900 μm. (F to I) Immunohistochemistry using antibodies against synapsin (F and G), and vesicular glutamate transporter VGlu1 (H and I) shows punctate staining patterns in the neuropil of both wild-type (F and H) and null mutant brains (G and I). Bar in panel I (for panels F to I), 20 μm.

also demonstrated that β-galactosidase staining was most intense over nuclei (Fig. 2E), consistent with the presence of a nuclear localization signal preceding the *lacZ* sequence. To further characterize the Nxph3-expressing cell populations, we performed double-labeling of sections from adult knock-in brains with a number of marker proteins. These experiments proved difficult, since (i) visualization of Nxph3-*lacZ* required long incubation in β-galactosidase staining solution as a first step, which reduces the fidelity of immunohistochemistry; and (ii) antibodies against β-galactosidase were not sensitive enough to allow reliable detection. In spite of these limitations, immunostaining with antibodies against GAD67 (Fig. 2F), parvalbumin, and calretinin (data not shown) demonstrated that Nxph3-positive cells (arrows) are not labeled as GABAergic neurons (arrowheads), suggesting that they are presumably excitatory neurons. To test if all Nxph3-positive cells in the cortex are subplate derived neurons, we probed for colocalization with an established marker protein, Tbr1 (5), demonstrating partial but not exclusive overlap during the early postnatal period (Fig. 2G and H). Since partial colocalization was also observed with neuropeptides, such as substance P and somatostatin (data not shown), Nxph3-expressing neurons appear as a nonuniform cell type, consistent with data showing that layer 6 contains a heterogenous population of neurons from dual origins that appear early during ontogenesis (10) and later develop corticothalamic or long intracortical connections (33).

Next, we investigated Nxph3 expression in the cerebellum and observed a remarkable regional specificity. Nxph3 was restricted mainly to lobules 9 and 10 of the cerebellar vermis (Fig. 1H and 2I), and no Nxph3-positive cells were found in the other parts. A higher magnification analysis showed that expression was most likely confined to the granule cell layer in these areas (Fig. 2J), suggesting that it occurs only in the non-GABAergic neurons of the cerebellum. To test directly if Nxph3 was also excluded from GABAergic neurons in the cerebellum, we performed double-labeling experiments with antibodies against GAD67, VGAT, and parvalbumin. These marker proteins stained all GABAergic neurons of the cerebellum but did not colocalize with Nxph3 (data not shown), consistent with the findings for the cortex and with the idea that Nxph3 expression does not identify a uniform cell type but may be functionally required in particular networks.

TABLE 1. General phenotypic characterization of neurexophilin 1 and 3 null-mutant mice[a]

Parameter	Result for genotype indicated (no. of animals tested)			
	Wild type	Nxph1 KO	Nxph3 KO	Nxph1 and 3 DKO
Survival (%)[b]	104 (332)	71 (76)	123 (132)	83 (29)
Body weight (g)[c]	23.6 ± 1.9(14)	21.4 ± 2.5(11)	23.5 ± 1.8(12)	22.1 ± 2.1(10)

[a] Data are means ± standard errors of the means (SEM). All animals used in this phenotypic analysis were littermate offspring from parents heterozygous for neurexophilin 1 and 3 and were generated by breeding the Nxph3 knockout reported in this study to the Nxph1 knockout published earlier (18).
[b] Percent of expected numbers (assuming Mendelian distribution) at 6 weeks of age demonstrating no reduction of viability in Nxph3-deficient mice.
[c] Body weight was measured in female offspring at 6 weeks of age. No significant differences were observed.

Nxph3 expression during development. To investigate if the restricted expression pattern of Nxph3 was the result of an ontogenetic down-regulation or if it was established early in development, we first confirmed by Northern blotting that Nxph3 is expressed at similar levels throughout postnatal development (Fig. 3A). Next, we explored β-galactosidase-labeled sections from knock-in mice of various ages. The two regions containing Nxph3-positive neurons in adult animals (Fig. 1 and 2) showed little variation in expression patterns during ontogenesis. Perinatally, Nxph3 was present in subplate cells of the cortex (Fig. 3B and C, arrows) that later develop into layer 6b neurons (Fig. 3D and E, arrows). Consistent with the delayed ontogenesis in the cerebellum, prominent Nxph3 expression started only at about P11 in lobules 9 and 10 (data not shown). In addition, the transiently expressing Nxph3 neurons that were found perinatally in the marginal zone (Fig. 3B and C, arrowheads) disappeared from layer 1 after the first postnatal week (Fig. 3D and E); those found during the first postnatal week in the molecular layer of the dentate gyrus (Fig. 4A and B, arrowheads) vanished after the second week (Fig. 4C and D). The time course and location of both populations were strongly indicative of Cajal-Retzius cells, suggesting that Nxph3 represents a novel marker for these transient neurons. To confirm their identity, double-labeling experiments for β-galactosidase and marker proteins reelin or calretinin were performed on sections from P7 knock-in mice (Fig. 4E and F, reelin; Fig. 4G and H, calretinin). The observed colocalization supports the hypothesis that transiently occurring Nxph3-positive cells in the dentate gyrus (Fig. 4E to H) and the marginal zone (data not shown) represent Cajal-Retzius neurons (5). In contrast, the Nxph3-positive, presumably subplate-derived layer 6b neurons were negative for reelin, consistent with published data (5).

Nxph3 is not required for normal brain architecture. The restricted distribution of Nxph3 is in contrast to that of its only known interaction partner, α-neurexins, which are essential for efficient neurotransmission at many types of synapses throughout the brain (21). To evaluate the role of Nxph3, we generated a knockout mouse line by breeding the floxed knock-in mice to a transgenic "deleter" strain (Fig. 5A), that expresses Cre recombinase early during development (EIIa-Cre$^{+/tg}$) (15). Nxph3 knockouts were viable and fertile with no obvious morbidity (Table 1). The evidence for complete deletion of Nxph3 by site-specific recombination rests on the absence of β-galactosidase activity (data not shown) and the absence of its mRNA (Fig. 5B). To show removal of protein, we crossed Nxph3 knockouts with null mutants of its companion, Nxph1 (18). This double knockout approach was necessary since antisera cross-reacted with both isoforms, which have similar molecular weights (20). In double knockouts deficient for both Nxph1 and Nxph3, a lack of both proteins was observed with α-latrotoxin pulldown experiments (Fig. 5C). Consistent with their presumably nonoverlapping distribution patterns (Fig. 1 to 4 and reference 26), double mutants exhibited no significant differences in mortality or body weight compared to Nxph3 single knockouts or to wild-type controls (Table 1). Immunoblots displayed no apparent upregulation of the respective other isoform (Fig. 5C and reference 18), suggesting that Nxph1 and Nxph3 act independently.

To test if the anatomy of Nxph3 mutant brains is normal, we examined serial sections from Nxph3-deficient and littermate control mice (Fig. 5D and E). However, no obvious abnormalities that would indicate a loss of Nxph3-positive neurons or mislayering in knockout brains, such as changes in cortical lamination or diminished lobules 9 or 10 in the cerebellum, could be uncovered. To probe for minor differences in brain architecture, we quantitated layer thickness and cell density in the cortical areas that show expression of Nxph3 in normal animals, but no changes could be detected for the knockouts (Table 2). As the tight binding of Nxph3 to α-neurexins may imply a role at synapses, we next investigated the distribution patterns of a number of marker proteins in the cerebral cortex, using antibodies against proteins present at excitatory or inhibitory synapses. However, no changes in overall intensity of labeling were found (data not shown; $n > 3$ mice for all marker proteins tested). In these experiments, we paid particular at-

TABLE 2. Quantitative structural analysis of the neocortical grey matter in Nxph3 knockout mice[a]

Parameter	Result for genotype indicated			P^d
	Wild type	Nxph3 knockout	Nxph3 knock-in	
Thickness (μm)[b]				
Total	841.5 ± 26.4	795.9 ± 31.5	760.6 ± 33.3	NS
Layer 5	189.5 ± 11.1	172.3 ± 10.1	179.6 ± 5.6	NS
Layer 6	252.6 ± 14.0	242.5 ± 10.4	218.9 ± 11.2	NS
Density (cells/mm^2)[c]	3,106 ± 241	3,299 ± 132	3,149 ± 147	NS

[a] Data are means ± SEM; $n = 3$ for each group. The wild-type and knockout animals used in this morphological analysis were littermates aged 5 to 6 weeks. Knock-in mice were derived from an independent mouse line; age- and gender-matched animals were used for the experiments. Several brain areas were investigated with Nissl-stained serial sections; numbers presented here are from the primary somatosensory cortex.
[b] Total thickness of area Par1 was measured along a perpendicular line from the Pia to the white matter.
[c] To avoid any bias towards the putative nature of the phenotype, all neuronal and glial cells were included.
[d] For statistical analysis, a two-sided ANOVA was used (GraphPad Prism software).

TABLE 3. Quantitative behavioral analysis of Nxph3 knockout mice[a]

Behavioral test	Result for genotype indicated (no. of animals tested)		*P*
	Wild type	Nxph3 KO	
Grip strength (pond)	114.8 ± 6.3 (10)	118.4 ± 5.9 (9)	NS
Open field			
Walking speed (cm/s)	6.5 ± 0.8 (6)	4.9 ± 0.8 (10)	NS
Total distance (m)	56.4 ± 6.5 (6)	42.5 ± 6.6 (10)	NS
Time in outfield (% of time)	83.7 ± 3.9 (6)	69.4 ± 6.6 (10)	NS
Time in center (% of time)	16.3 ± 3.8 (6)	30.2 ± 6.9 (10)	NS
Time in corners (% of time)	44.2 ± 2.6 (6)	36.7 ± 6.5 (10)	NS
Light-dark avoidance			
Light compartment (% of time)	75.6 ± 9.0 (6)	68.4 ± 7.6 (10)	NS
Dark compartment (% of time)	24.4 ± 9.0 (6)	31.6 ± 7.6 (10)	NS
Compartment changes (no.)	26.7 ± 11.8 (6)	23.6 ± 4.6 (10)	NS
Two-way active avoidance (% active avoidance reactions)			
Day 1	7.0 ± 1.1 (10)	5.4 ± 1.8 (9)	NS
Day 2	30.6 ± 6.4 (10)	17.6 ± 4.3 (9)	NS
Day 3	59.5 ± 7.9 (10)	45.5 ± 9.4 (9)	NS
Day 4	67.4 ± 7.1 (10)	61.5 ± 10.8 (9)	NS
Day 5	79.8 ± 3.9 (10)	72.1 ± 8.3 (9)	NS
Morris water maze			
Swim path length (m)			
Day 1 (acquisition)	11.6 ± 0.9 (11)	10.7 ± 1.0 (13)	NS
Day 2 (acquisition)	9.1 ± 0.9 (11)	7.1 ± 0.9 (13)	NS
Day 3 (acquisition)	7.6 ± 0.8 (11)	6.9 ± 0.8 (13)	NS
Day 4 (reversal)	7.2 ± 0.9 (11)	7.9 ± 0.8 (13)	NS
Day 5 (reversal)	7.5 ± 0.9 (11)	7.6 ± 0.8 (13)	NS
Escape latency (s)			
Day 1 (acquisition)	73.4 ± 5.9 (11)	55.8 ± 5.3 (13)	0.028
Day 2 (acquisition)	62.1 ± 6.0 (11)	34.6 ± 4.2 (13)	0.0002
Day 3 (acquisition)	49.3 ± 4.8 (11)	32.6 ± 3.5 (13)	0.0048
Day 4 (reversal)	51.2 ± 5.5 (11)	39.9 ± 4.0 (13)	NS
Day 5 (reversal)	53.1 ± 5.2 (11)	39.2 ± 3.7 (13)	0.027

[a] Data are means ± SEM. All animals used in the behavioral analysis were littermates from heterozygous parents in a mixed 129SvJ × C57BL/6 × FVB background. Exact conditions of tests are described in Materials and Methods. NS, not significant.

tention to the punctate-like distribution pattern characteristic of many synaptic proteins. As demonstrated by the virtually identical appearance of labeling for synapsin (Fig. 5F and G), the vesicular glutamate (Fig. 5H and I) and GABA (data not shown) transporters, and the cytosolic Ca^{2+}-binding protein parvalbumin (data not shown), no morphological differences between wild-type and KO brains were observed.

Nxph3-deficient mice display a distinct behavioral phenotype. In the absence of structural phenotype, we addressed the functional significance of Nxph3 in brain by analyzing the behavior of knockout mice. Given the highly restricted distribution of Nxph3, we applied such a "top-down" strategy in order to circumvent problems that would be associated with a classical lack-of-function analysis, using, e.g., electrophysiological methods (21).

To achieve an unbiased behavioral assessment, an investigator unaware of the genotypes subjected mice to a comprehensive battery of behavioral paradigms (22, 27) as outlined in Materials and Methods. While Nxph3 knockouts performed well in most tests, with results indistinguishable from those of the littermate controls (Table 3), their abilities were altered specifically in sensorimotor gating (Fig. 6) and in motor coordination (Fig. 7).

The acoustic startle response is an unconditioned reflex to an intense noise stimulus. As shown in Fig. 6A, the magnitude of the acoustic startle response in Nxph3 knockout mice ($g = 27.97 \pm 2.3$; $n = 13$) was increased twofold compared to controls ($g = 13.05 \pm 2.6$; $n = 12$; $F_{1,23} = 18.2$; $P = 0.0003$). In normal subjects of many species, including humans and mice, the acoustic startle response is strongly reduced when a prepulse stimulus is presented before the main startle stimulus (32). The level of this PPI in Nxph3 knockout and littermate control mice, expressed as the percent reduction of the baseline startle response, is shown in Fig. 6B. At all intensities tested, a significant reduction of PPI was apparent in Nxph3 mutant mice (e.g., 44.7% PPI at 94 dB; $n = 13$), whereas controls displayed normal levels of suppression (e.g., 69.6% PPI at 94 dB; $n = 12$; $F_{1,23} = 26.9$; $P < 0.0001$).

Motor coordination was tested using a rotarod apparatus, where the latency to fall off the rotating drum was measured (Fig. 7A). During the two training sessions, knockout animals ($n = 17$) were not able to maintain their balance for the same lengths of time as the control group ($n = 12$). The overall genotype influence was significant ($F_{1,27} = 8.12$; $P = 0.0083$, repeated measures ANOVA), as was the genotype influence for the first training session ($F_{1,27} = 10.204$; $P = 0.0035$) and at the 16-rpm ($F_{1,27} = 5.68$; $P = 0.0244$), 24 rpm ($F_{1,27} = 6.26$; $P = 0.0187$), and 32 rpm ($F_{1,27} = 5.483$; $P = 0.0268$) fixed speed trials. The impaired motor coordination, however, was not due to an overall dysfunction of locomotor behavior; natural roaming and exploratory behavior, as assessed in the open field, failed to show significant differences (Table 3). Similarly, even in more physically challenging paradigms, such as the Morris water maze task, Nxph3 knockout mice were not only able to

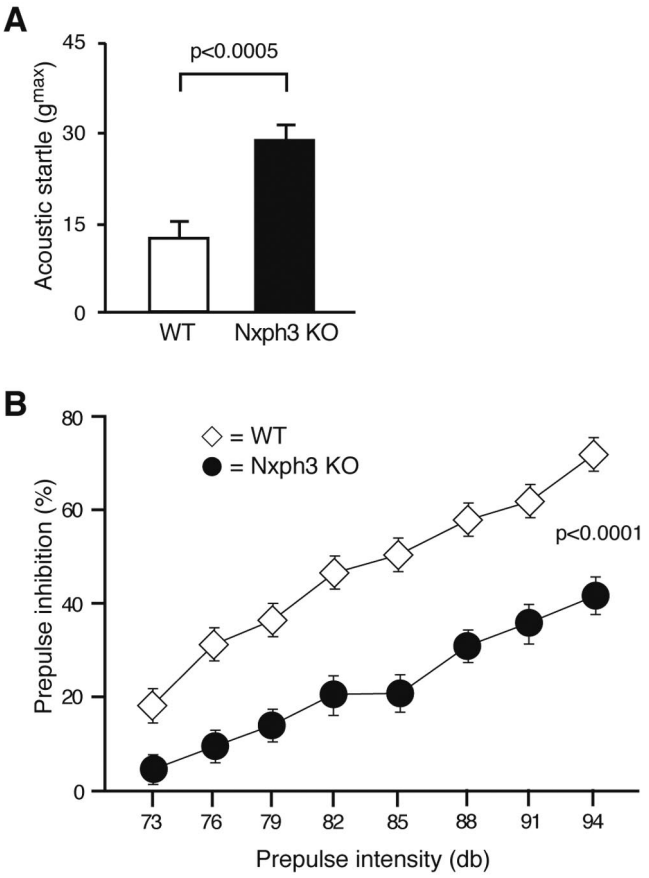

FIG. 6. Impaired sensorimotor gating in Nxph3 knockout mice. (A) Amplitudes of the acoustic startle response were significantly increased in Nxph3 knockout mice (KO; $n = 13$) compared to littermate WT controls ($n = 12$). (B) Prepulse inhibition of the startle response was measured at increasing intensities of the warning tone (prepulse). Compared to WT littermate animals ($n = 12$), Nxph3-deficient mice (Nxph3 KO; $n = 13$) display a significantly reduced inhibition by the prepulse at all prepulse intensities tested. Data are expressed as means ± SEM.

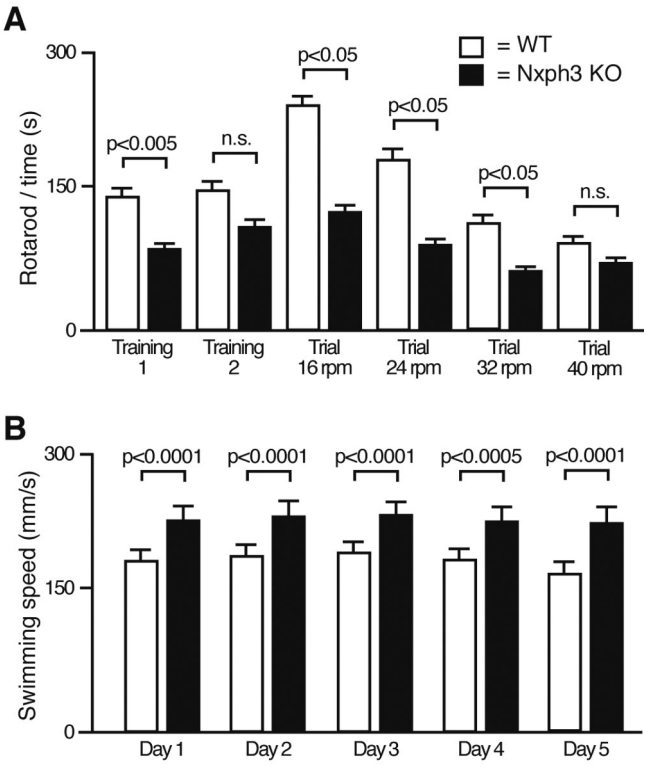

FIG. 7. Motor coordination defects in Nxph3 mutants. (A) The ability for motor coordination and balance of WT ($n = 12$) and Nxph3 knockout mice (Nxph3 KO; $n = 17$) was tested with a rotarod apparatus. During accelerating training sessions and trials with constant speed (trials at 16, 24, and 32 rpm), knockout animals exhibited significantly shorter latencies to fall of the rotating drum. n.s., not significant. (B) Measurements of swimming speed during the Morris water maze task demonstrated that Nxph3 knockout mice ($n = 13$) do not suffer from an overall impaired locomotor ability but can outperform even their littermate controls ($n = 11$). Data are expressed as means ± SEM.

efficiently use the remote visual cues (Table 3) but also displayed a good swimming performance, as evidenced by unchanged swim path lengths (Table 3) and even better-than-control swimming speeds (Fig. 7B). Nxph3-deficient mice ($n = 13$) swam faster ($F_{1,145} = 37.221$; $P < 0.0001$) and thus showed shorter escape latencies (Table 3) than littermate controls ($n = 11$).

DISCUSSION

We examined the distribution and function of neurexophilin 3 (Nxph3), a specific extracellular ligand of the cell-surface molecules α-neurexins. Neurexins are receptors for α-latrotoxin, which causes massive neurotransmitter release from presynaptic terminals (8, 30, 36, 37), and they are required for neurotransmission by affecting synaptic Ca^{2+}-channels and *N*-methyl-D-aspartate (NMDA) receptors (12, 21). The knock-in approach reported here revealed that Nxph3 is expressed mostly in neurons in the deep cortical layers (Fig. 1 and 2), regions of the vestibulocerebellum (Fig. 1 and 2), and Cajal-Retzius cells during development (Fig. 3 and 4). An identical expression pattern has not been reported for any other protein. The Nxph3-positive subplate-derived layer 6b neurons and Cajal-Retzius cells are early born neurons that take part in primordial neuronal circuits (1). While the layer 6 neurons are involved in the growth and differentiation of thalamocortical, corticothalamic, and callosal axons (10), Cajal-Retzius cells regulate cortical layering and organize entorhinal connections in the hippocampus (5). Colabeling experiments demonstrated that Nxph3 was a novel marker for those neurons involved in cortical maturation of both the marginal zone and the hippocampus (5), although colocalization was only partial. The restricted pattern of Nxph3 was surprising, since the distribution of Nxph3 neither overlaps nor is complementary to that of Nxph1, the only other α-neurexin-binding neurexophilin in mice, which occurs in interneurons of many brain regions (26). Although Nxph3 is expressed exclusively in non-GABAergic neurons, the distribution of Nxph3 is even more restricted than that of Nxph1, suggesting that Nxph1 or Nxph3-positive neurons together constitute only a minority of neurons in the brain. Since isoforms of α-neurexins that are capable of binding all neurexophilins (18) are present in most neurons (35), this disparity indicates that the Nxph/α-neurexin binding is not a ubiquitous complex, but represents a facultative interaction used only at distinct synapses.

The functional significance of Nxph3 in null mutant mice generated by *Cre/loxP* mediated deletion was tested (Fig. 5). In contrast to knockout mice of colocalized marker proteins reelin and Tbr1 (5, 9), the deletion of Nxph3 did not cause a structural phenotype (Fig. 5; Table 2). Instead, a thorough behavioral analysis of knockout mice revealed the importance of Nxph3 for brain function. Nxph3 knockouts displayed specific impairments in sensorimotor gating and motor coordination tasks (Fig. 6 and 7), while they performed normally in a large number of other behavioral tests (Table 3). Inadequate processing of sensory information as tested for in prepulse inhibition of the startle response (PPI) is a diagnostic indicator of several neuropsychiatric disorders (32). Published evidence of regions implicated in the regulation of PPI include deep cortical layers, the hippocampus, and the basolateral nucleus of the amygdala (32). The acoustic startle response itself is mediated by a neuronal pathway located in the ponto-medullary brainstem and can be evoked by electrical stimulation of the amygdala (2, 13), and PPI can be reduced by local infusion of NMDA receptor antagonists (32). Unlike the difference in structural phenotypes between Nxph3 and reelin-deficient mice, heterozygous reeler mice that lack about 50% of reelin in their Cajal-Retzius cells show a strongly reduced PPI, similar to results seen with Nxph3 null mutants (34). Since those regions and cell types implicated in startle response contained many Nxph3-expressing neurons (Fig. 1 to 4), we speculate that synaptic and/or cellular malfunctions cause the behavioral phenotype of altered startle response and PPI (Fig. 6). Moreover, huntingtin transgenic mice that express expanded glutamine repeats predominantly in neurons of layer 6 and in the granule cells of the cerebellum display a combination of behavioral defects similar to those demonstrated here for Nxph3 knockout animals, i.e., reduced PPI and abnormalities in motor coordination (3, 14). Correspondingly, the impaired motor coordination observed with the Nxph3 knockouts (Fig. 7) may be attributed to a malfunctioning of granule cells. These cells normally express Nxph3 (Fig. 1 and 2) and constitute a major component of the mossy fiber-parallel fiber system in the vestibulocerebellum that generates fine control of movement (16). Taken together, our study data indicate an important role for Nxph3 in the brain. Remaining open, however, are the questions of whether this function necessarily involves Nxph3 tightly bound to synaptic α-neurexins (18, 20, 26) and whether Nxphs are actually involved in synaptic transmission as locally and temporally restricted modulator molecules.

ACKNOWLEDGMENTS

We thank T. C. Südhof, C. Shatz, J. R. Wolff and M. Wines-Samuelson for discussions; S. Gerke and K. Sowa for excellent technical assistance; N. Brose (Göttingen, Germany) for providing EIIa $Cre^{+/tg}$ mice, A. Petrenko (New York) for recombinant α-latrotoxin, and J. Rubenstein (UCSF) and M. Frotscher (Freiburg, Germany) for antibodies to Tbr1 and reelin, respectively.

This study was supported by grants from the Deutsche Forschungsgemeinschaft (DFG; grant SFB 406-C9 to M.M.) and a Georg Christoph Lichtenberg Stipend (Ministry for Science and Culture of Lower Saxony, Germany) to M.A.

REFERENCES

1. **Arber, S.** 2004. Subplate neurons: bridging the gap to function in the cortex. Trends Neurosci. **27:**111–113.
2. **Carlson, S., and J. F. Willott.** 1998. Caudal pontine reticular formation of C57BL/6J mice: responses to startle stimuli, inhibition by tones, and plasticity. J. Neurophysiol. **79:**2603–2614.
3. **Carter, R. J., L. A. Lione, T. Humby, L. Mangiarini, A. Mahal, G. P. Bates, S. B. Dunnett, and A. J. Morton.** 1999. Characterization of progressive motor deficits in mice transgenic for the human Huntington's disease mutation. J. Neurosci. **19:**3248–3257.
4. **Dean, C., F. G. Scholl, J. Choih, S. DeMaria, J. Berger, E. Isacoff, and P. Scheiffele.** 2003. Neurexin mediates the assembly of presynaptic terminals. Nat. Neurosci. **6:**708–716.
5. **Del Rio, J. A., B. Heimrich, H. Super, V. Borrell, M. Frotscher, and E. Soriano.** 1996. Differential survival of Cajal-Retzius cells in organotypic cultures of hippocampus and neocortex. J. Neurosci. **16:**6896–6907.
6. **Dymecki, S. M.** 1996. Flp recombinase promotes site-specific DNA recombination in embryonic stem cells and transgenic mice. Proc. Natl. Acad. Sci. USA **93:**6191–6196.
7. **Feliciangeli, S., P. Kitabgi, and J. N. Bidard.** 2001. The role of dibasic residues in prohormone sorting to the regulated secretory pathway. A study with proneurotensin. J. Biol. Chem. **276:**6140–6150.
8. **Geppert, M., M. Khvotchev, V. Krasnoperov, Y. Goda, M. Missler, R. E. Hammer, K. Ichtchenko, A. G. Petrenko, and T. C. Südhof.** 1998. Neurexin I alpha is a major alpha-latrotoxin receptor that cooperates in alpha-latrotoxin action. J. Biol. Chem. **273:**1705–1710.
9. **Graf, E. R., X. Zhang, S. X. Jin, M. W. Linhoff, and A. M. Craig.** 2004. Neurexins induce differentiation of GABA and glutamate postsynaptic specializations via neuroligins. Cell **119:**1013–1026.
10. **Hevner, R. F., L. Shi, N. Justice, Y. Hsueh, M. Sheng, S. Smiga, A. Bulfone, A. M. Goffinet, A. T. Campagnoni, and J. L. Rubenstein.** 2001. Tbr1 regulates differentiation of the preplate and layer 6. Neuron **29:**353–366.
11. **Ichtchenko, K., Y. Hata, T. Nguyen, B. Ullrich, M. Missler, C. Moomaw, and T. C. Südhof.** 1995. Neuroligin 1: a splice site-specific ligand for beta-neurexins. Cell **81:**435–443.
12. **Kattenstroth, G., E. Tantalaki, T. C. Sudhof, K. Gottmann, and M. Missler.** 2004. Postsynaptic *N*-methyl-D-aspartate receptor function requires alpha-neurexins. Proc. Natl. Acad. Sci. USA **101:**2607–2612.
13. **Koch, M.** 1999. The neurobiology of startle. Prog. Neurobiol. **59:**107–128.
14. **Laforet, G. A., E. Sapp, K. Chase, C. McIntyre, F. M. Boyce, M. Campbell, B. A. Cadigan, L. Warzecki, D. A. Tagle, P. H. Reddy, C. Cepeda, C. R. Calvert, E. S. Jokel, G. J. Klapstein, M. A. Ariano, M. S. Levine, M. DiFiglia, and N. Aronin.** 2001. Changes in cortical and striatal neurons predict behavioral and electrophysiological abnormalities in a transgenic murine model of Huntington's disease. J. Neurosci **21:**9112–9123.
15. **Lakso, M., J. G. Pichel, J. R. Gorman, B. Sauer, Y. Okamoto, E. Lee, F. W. Alt, and H. Westphal.** 1996. Efficient in vivo manipulation of mouse genomic sequences at the zygote stage. Proc. Natl. Acad. Sci. USA **93:**5860–5865.
16. **Llinas, R., and K. Walton.** 1998. Cerebellum, p. 255–288. *In* G. Shepherd (ed.), The synaptic organization of the brain. Oxford University Press, New York, N.Y.
17. **Missler, M.** 2003. Synaptic cell adhesion goes functional. Trends Neurosci. **26:**176–178.
18. **Missler, M., R. E. Hammer, and T. C. Südhof.** 1998. Neurexophilin binding to α-neurexins. A single LNS domain functions as an independently folding ligand-binding unit. J. Biol. Chem. **273:**34716–34723.
19. **Missler, M., and T. C. Südhof.** 1998. Neurexins: three genes and 1001 products. Trends Genet. **14:**20–26.
20. **Missler, M., and T. C. Südhof.** 1998. Neurexophilins form a conserved family of neuropeptide-like glycoproteins. J. Neurosci. **18:**3630–3638.
21. **Missler, M., W. Zhang, A. Rohlmann, G. Kattenstroth, R. E. Hammer, K. Gottmann, and T. C. Sudhof.** 2003. α-Neurexins couple Ca^{2+} channels to synaptic vesicle exocytosis. Nature **424:**939–948.
22. **Montag-Sallaz, M., and D. Montag.** 2003. Severe cognitive and motor coordination deficits in tenascin-R-deficient mice. Genes Brain Behav. **2:**20–31.
23. **Mountford, P. S., and A. G. Smith.** 1995. Internal ribosome entry sites and dicistronic RNAs in mammalian transgenesis. Trends Genet. **11:**179–184.
24. **Petrenko, A. G., V. A. Kovalenko, O. G. Shamotienko, I. N. Surkova, T. A. Tarasyuk, Y. Ushkaryov, and E. V. Grishin.** 1990. Isolation and properties of the alpha-latrotoxin receptor. EMBO J. **9:**2023–2027.
25. **Petrenko, A. G., V. D. Lazaryeva, M. Geppert, T. A. Tarasyuk, C. Moomaw, A. V. Khokhlatchev, Y. A. Ushkaryov, C. Slaughter, I. V. Nasimov, and T. C. Südhof.** 1993. Polypeptide composition of the α-latrotoxin receptor. High affinity binding protein consists of a family of related high molecular weight polypeptides complexed to a low molecular weight protein. J. Biol. Chem. **268:**1860–1867.
26. **Petrenko, A. G., B. Ullrich, M. Missler, V. Krasnoperov, T. W. Rosahl, and T. C. Südhof.** 1996. Structure and evolution of neurexophilin. J. Neurosci. **16:**4360–4369.
27. **Rogers, D. C., E. M. Fisher, S. D. Brown, J. Peters, A. J. Hunter, and J. E. Martin.** 1997. Behavioral and functional analysis of mouse phenotype: SHIRPA, a proposed protocol for comprehensive phenotype assessment. Mamm. Genome **8:**711–713.
28. **Scheiffele, P.** 2003. Cell-cell signaling during synapse formation in the CNS. Annu. Rev. Neurosci. **26:**485–508.
29. **Stricklett, P. K., R. D. Nelson, and D. E. Kohan.** 1998. Site-specific recom-

bination using an epitope tagged bacteriophage P1 Cre recombinase. Gene **215:**415–423.
30. **Sugita, S., M. Khvochtev, and T. C. Südhof.** 1999. Neurexins are functional alpha-latrotoxin receptors. Neuron **22:**489–496.
31. **Sugita, S., F. Saito, J. Tang, J. Satz, K. Campbell, and T. C. Sudhof.** 2001. A stoichiometric complex of neurexins and dystroglycan in brain. J. Cell Biol. **154:**435–445.
32. **Swerdlow, N. R., M. A. Geyer, and D. L. Braff.** 2001. Neural circuit regulation of prepulse inhibition of startle in the rat: current knowledge and future challenges. Psychopharmacology (Berlin) **156:**194–215.
33. **Tombol, T., F. Hajdu, and G. Somogyi.** 1975. Identification of the Golgi picture of the layer VI cortic-geniculate projection neurons. Exp. Brain Res. **24:**107–110.
34. **Tueting, P., E. Costa, Y. Dwivedi, A. Guidotti, F. Impagnatiello, R. Manev, and C. Pesold.** 1999. The phenotypic characteristics of heterozygous reeler mouse. Neuroreport **10:**1329–1334.
35. **Ullrich, B., Y. A. Ushkaryov, and T. C. Südhof.** 1995. Cartography of neurexins: more than 1000 isoforms generated by alternative splicing and expressed in distinct subsets of neurons. Neuron **14:**497–507.
36. **Ushkaryov, Y. A., A. G. Petrenko, M. Geppert, and T. C. Südhof.** 1992. Neurexins: synaptic cell surface proteins related to the alpha- latrotoxin receptor and laminin. Science **257:**50–56.
37. **Valtorta, F., L. Madeddu, J. Meldolesi, and B. Ceccarelli.** 1984. Specific localization of the alpha-latrotoxin receptor in the nerve terminal plasma membrane. J. Cell Biol. **99:**124–132.
38. **Whishaw, I. Q., F. Haun, and B. Kolb.** 1999. Analysis of behaviour in laboratory rodents, p. 1243–1275. *In* U. Windhorst and H. Johansson (ed.), Modern techniques in neuroscience. Springer, Berlin, Germany.
39. **Wolfer, D. P., and H. P. Lipp.** 1992. A new computer program for detailed off-line analysis of swimming navigation in the Morris water maze. J. Neurosci. Methods **41:**65–74.
40. **Zhang, W., A. Rohlmann, V. Sargsyan, G. Aramuni, R. E. Hammer, T. C. Sudhof, and M. Missler.** 2005. Extracellular domains of alpha-neurexins participate in regulating synaptic transmission by selectively affecting N- and P/Q-type Ca^{2+} channels. J. Neurosci. **25:**4330–4342.